SOIL MECHANICAL PROPERTIES AT THE INSIGHT LANDING SITE ON MARS. E. Marteau[1], M. Golombek[1], C. Vrettos[2], J.B. Garvin[3], and N.R. Williams[1]. [1]Jet Propulsion Laboratory, California Institute of Technology, Pasadena, CA (eloise.marteau@jpl.nasa.gov); [2]Technical University of Kaiserlautern, Kaiserlautern, Germany; [3]NASA Goddard Space Flight Center, Greenbelt, MD.

Introduction: The NASA InSight lander [1] has been operating on Mars since November 26, 2018. InSight is equipped with a four degree-of-freedom robotic arm, two color cameras (one mounted on the robotic arm and one mounted on the lander), and several science instruments. The robotic arm end-effector includes a scoop which is used to interact with surface material.

Background: Observations at the InSight landing site suggest a subsurface geological structure consisting of dust (microns), over unconsolidated sand (~1 cm), underlain by duricrust (7-20 cm), with a fined grained regolith layer of unconsolidated sand and sparse rocks underneath [2,3].

Images of the pits that formed beneath the lander during touchdown and around the mole (part of the Heat Flow and Physical Properties Package, HP^3) during hammering show steep walls (Figure 1). The pit slope angles are much greater than the angle of repose and nearly vertical in the case of the HP^3 mole pit, which implies that the material has some cohesion. Stability analysis based solely on the slope angle of the pits excavated by the retrorockets beneath the lander yield a minimum cohesion > 0.02 kPa, as reported in [2].

Soil mechanics experiments aiming at characterizing the cohesion and internal friction angle have been previously conducted on Mars. Of particular interest are the investigations performed by the Viking and Phoenix lander robotic arms [4,5]. At the InSight landing site, the pit that formed around the HP^3 mole offers a unique opportunity to combine slope stability analysis with measurements of robotic arm forces at the end-effector and images to estimate the mechanical properties of the martian soil.

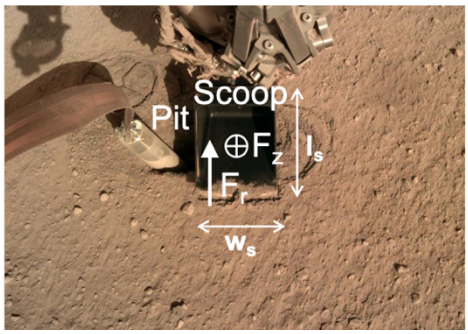

Figure 1: Annotated image of the scoop interacting with the soil near the HP^3 pit. Direction of the vertical force F_z and radial force F_r during the preload. w_s and l_s are, respectively, the width and length of the scoop.

Method: In considering the problem of slope stability, we assume plane strain conditions, that the material is homogeneous, and that a Mohr-Coulomb failure criterium is satisfied along the failure plane. The slope stability is studied using Culmann's method, which is known to give reasonably accurate results if the slope is nearly vertical [6]. Culmann's method assumes that the critical failure surface is a straight-line plane passing through the toe of the slope. The method is based on the assumption that the failure of a slope occurs along a plane when the average shear stress tending to cause the slip exceeds the shear strength of the soil.

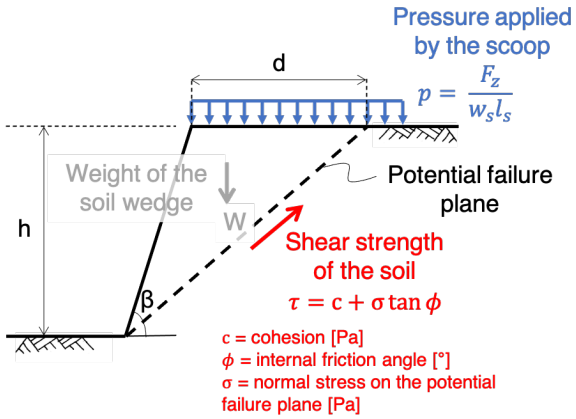

Figure 2: Slope stability analysis – Culmann's method.

Figure 2 shows a finite slope of height h. The slope rises at an angle β with the horizontal and the potential failure plane is shown as a dashed line. The slope failure can occur by the movement of the soil above the potential failure plane from right to left. The soil shear strength τ along the failure surface is defined by the Mohr-Coulomb equation as: $\tau = c + \sigma \tan \phi$. In this equation, σ is the normal stress on the potential failure plane, ϕ is the internal friction angle, and c is the cohesion. The method considers that static equilibrium conditions are satisfied and provides a relationship between the resisting force (i.e., the shear strength τ of the soil along the failure surface) and the driving forces tending to cause the slip (i.e., the weight W of the failing soil wedge and the force P applied by the scoop). As a result, a closed-form expression for the cohesion c can be derived:

$$c = \frac{(W + P)(\cos \phi - \cos \beta)}{2h \cos \phi} \quad (1)$$

The weight W of the wedge is given by:

$$W = \frac{1}{2}\rho g h^2 \frac{\sin\left(\frac{\beta-\phi}{2}\right)}{\sin\left(\frac{\beta+\phi}{2}\right)\sin\beta} \quad (2)$$

where ρ is the bulk density of the soil and g is the gravitational acceleration. The force P acting on the wedge due to the scoop load is given by:

$$P = pd = \frac{h\,F_z}{w_s\,l_s}\left[\cot\left(\frac{\beta+\phi}{2}\right) - \cot\beta\right] \quad (3)$$

where, as depicted in Figure 2, p is the uniform pressure exerted by the scoop, d is the length of wedge, w_s = 0.071 m is the width of the scoop, l_s = 0.092 m is the length of the scoop, and F_z is the vertical component of the scoop force .

Results: On Sol 240, the flat part of the robotic arm scoop was used to apply a preload at the edge of the HP^3 mole pit in an attempt to cause failure of the western wall, as shown in Figure 1. The robotic arm flight software [7] determined that the force applied by the scoop was F_z = 59 N in the vertical direction and F_r = 40 N in the radial direction. Such force did not cause slope failure (Figure 3a). It is worth noting that, without a slope failure, equation (1) provides a lower bound estimate of the cohesion. The force F_r, which acts away from the lander, does not affect the stability and only the vertical force F_z is considered in the analysis.

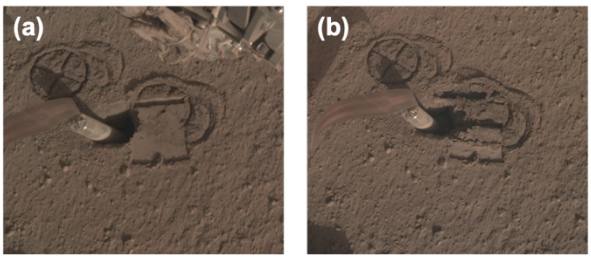

Figure 3: Images of robotic arm scoop interactions with the surface material near the HP^3 mole pit. (a) After a flat push on Sol 240. (b) After a tip push on Sol 250.

A topographic map of the HP^3 pit was used to measure the slope inclination angle β = 80° and height h = 0.05 m. Minimum estimates of the cohesion obtained using equation (1) are calculated for a range of presumed internal friction angles ϕ between 30° and 40° and bulk densities ρ between 1200 kg/m^3 and 1600 kg/m^3 [8]. The results indicate that a minimum cohesion c between 1.5 and 1.9 kPa is required for the slope to be marginally stable when a force P is applied by the flat part of the robotic arm scoop.

Subsequently, on Sol 250, the tip of the scoop was pushed into the soil near the HP^3 mole pit. The force applied by the tip of the scoop was F_z = 50 N. The arm interaction with the surface resulted in the failure of a soil wedge (Figure 3b). High-fidelity Digital Elevation Models (DEM) obtained using Structure-from-Motion (SFM) computation [9] provided information on the geometry of the failure wedge, i.e., a failure angle of 35° and a height of 0.013 m. If we use this finding in conjunction with equation (1), and take into account the lower bound estimate of the cohesion obtained from the flat push on Sol 240, we obtain a cohesion c between 2 and 14.5 kPa for values of the internal friction angle ϕ between 30° and 35°, as depicted by Figure 4.

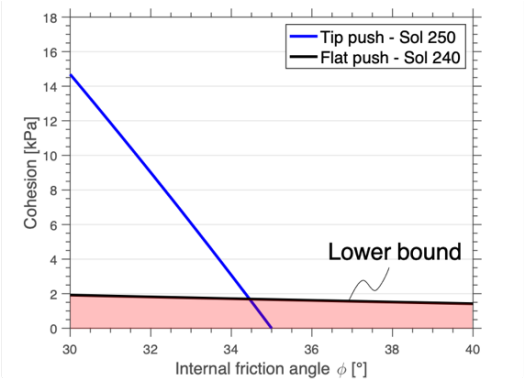

Figure 4: Cohesion c as a function of the internal friction angle ϕ for the scoop flat push on Sol 240 and the tip push on Sol 250. The red shaded region represents the range of disallowed values for c.

Discussion: Cohesions of 2-14 kPa for InSight duricrust are similar to relatively strong, blocky, indurated soil at Viking Lander 2 and the range of densities and internal friction angles are similar to other soils on Mars [4]. In the laboratory, tests using the HP3 mole showed the formation of pits in simulants with cohesions of 2.5-12.5 kPa [10]. The effect of uncertainty in the input parameters was explored using a sensitivity analysis. Results show that the failure angle, which is a function of the internal friction angle and the slope inclination angle, has the most effect on the cohesion value, while variations in slope height, soil bulk density and vertical force applied do not greatly influence the cohesion estimate. Finally, future studies may further characterize the difference in cohesion and internal friction angle estimates obtained with 2D and 3D slope stability analyses.

References: [1] Banerdt W.B. et al. (2020) *Nat. Geosci*, *12*, 183-189. [2] Golombek M. et al. (2020) *Nat Commun*, *11*, 1014. [3] Hudson T.L. et al. (2020) 51st *LPSC,* Abstract #1217. [4] Moore H.J. et al. (1987) *U.S. Geol. Surv. Prof. Pap., 1389*, 222. [5] Shaw A. et al. (2009) *JGR, 114*, E00E05. [6] Scott R.F. (1963) *Principles of Soil Mechanics*, Addison-Wesley Publishing Co. [7] Trebi-Ollennu A. et al. (2018) *Space Sci. Rev., 214*, 93. [8] Grott M. et al., this issue. [9] Garvin J.B. et al. (2019) 50th *LPSC,* Abstract #2132. [10] Delage P. et al. (2017) *Space Sci. Rev., 211*, 191.